

# Emergent Hawking Radiation and Quantum Sensing in a Quenched Chiral Spin Chain

Nitesh Jaiswal<sup>1,\*</sup> and S. Shankaranarayanan<sup>1,†</sup>

<sup>1</sup>*Department of Physics, Indian Institute of Technology Bombay, Mumbai 400076, India*

## Abstract

We investigate the emergence and detection of Hawking radiation (HR) in a 1D chiral spin chain model, where the gravitational collapse is simulated by a sudden quantum quench that triggers a horizon-inducing phase transition. While our previous work [1] established that this model mimics BH formation conditions even when the Hoop conjecture is seemingly violated, we here focus on the resulting stationary radiation spectrum and its detectability. By mapping the spin chain dynamics to a Dirac fermion in a curved  $(1+1)$ -dimensional spacetime, we analyze the radiation using two complementary approaches: field-theoretic modes and operational quantum sensors. First, using localized Gaussian wave packets to model realistic detectors, we find that the radiation spectrum exhibits deviations from the ideal Planckian form, analogous to frequency-dependent greybody factors, while retaining robust Poissonian statistics that signal the loss of formation-scale information. Second, we introduce a qubit coupled to the chain as a stationary Unruh-DeWitt detector. We demonstrate that the qubit functions as a faithful quantum sensor of the Hawking temperature only in the weak-coupling regime, where its population dynamics are governed solely by the bath spectral density. In the strong-coupling limit, the probe thermalizes with the global environment, obscuring the horizon-induced thermal signature. These results provide a clear operational protocol for distinguishing genuine analog HR from environmental noise in quantum simulation platforms.

---

\* [niteshphy@iitb.ac.in](mailto:niteshphy@iitb.ac.in)

† [shanki@iitb.ac.in](mailto:shanki@iitb.ac.in)

*Introduction:* A central challenge in semiclassical and quantum gravity is the direct experimental verification of Hawking radiation (HR) [2–10]. While astrophysical observations, such as strong-field gravitational lensing, provide critical probes of the near-horizon geometry of black holes (BHs) [11, 12], the quantum dynamics of the horizon itself remain obscured by the weakness and delocalization of the radiation. Analogue gravity platforms have emerged as a powerful tool, as they enable controlled access to near-horizon quantum effects in laboratory settings ranging from fluids to optical systems [13–17].

To extract these elusive signatures from the background of a many-body system, we turn to the paradigm of *quantum sensing* [18–22]. Controlled spin-1/2 particles (qubits) have established themselves as highly sensitive probes of complex quantum environments, underpinning modern sensing technologies across molecular, atomic, and solid-state systems [18]. When coupled to an external bath, a qubit’s decoherence dynamics and population relaxation are governed by the spectral properties of the environment [23]. This allows for the precise extraction of noise spectra [24, 25] and Hamiltonian parameters [18] solely through measurements on the two-level probe.

Motivated by these capabilities, we employ a qubit as a stationary detector — analogous to an Unruh-DeWitt detector — to probe the analogous radiation in the chiral spin chain. In our previous work, we established that the chiral spin chain Hamiltonian can mimic gravitational collapse, satisfying black hole formation conditions even when the Hoop conjecture is violated [1]. In the present work, we focus on the implications for HR. Specifically, we investigate how the qubit’s decoherence profile encodes the emergent thermal features of the horizon.

Our analysis proceeds in two steps. First, we examine the radiation spectrum directly using both idealized plane waves and physically realistic Gaussian wave packets. We show that while plane waves recover the standard thermal spectrum, localized packets reveal deviations akin to greybody factors [26, 27], challenging the notion of HR as information-free. Second, we determine the operational conditions for detecting this temperature. We demonstrate that a qubit acts as a *faithful thermometer* only in the weak-coupling regime, whereas strong coupling leads to thermalization with the bulk environment rather than the horizon. Finally, we discuss the statistical nature of the emission, showing that the radiation remains Poissonian regardless of the geometric “Hoop” history, suggesting a universal erasure of formation scale information in the Hawking regime.

Model setup: To explore the dynamics of HR, we model the gravitational collapse as a sudden quantum quench [28–32]. We model the transition from a pre-horizon mass distribution to a BH using a time-dependent Hamiltonian  $H(t)$ . We assume the system initially evolves under a background Hamiltonian  $H_0$  (representing the pre-collapse phase) and undergoes a sudden change at  $t = t_0$  representing the formation of the horizon:

$$H(t) = H_0 + \Theta(t - t_0)H_h, \quad (1)$$

where  $\Theta(t - t_0)$  is the Heaviside step function and  $H_h$  denotes horizon-inducing dynamics and the probe interaction. In our analogue model, the pre-horizon regime is governed by the standard  $XX$  spin chain, given by [1]:

$$H_0 \equiv H_{XX} = - \sum_{j=1}^N (\mathcal{U}/2) (\sigma_j^x \sigma_{j+1}^x + \sigma_j^y \sigma_{j+1}^y), \quad (2)$$

where  $\sigma_j^\alpha$  are Pauli operators at site  $j$  satisfying periodic boundary conditions, and  $\mathcal{U}$  is the nearest-neighbor coupling strength. For  $t \geq t_0$ , the BH formation is captured by the activation of the chirality term  $H_\chi$  and the coupling to an external probe  $H_I$ . The quench Hamiltonian is defined as  $H_h = H_\chi + H_I$ . The chirality term is:

$$H_\chi = \sum_{j=1}^N (v/4) \chi_j, \quad (3)$$

where  $\chi_j = \vec{\sigma}_j \cdot (\vec{\sigma}_{j+1} \times \vec{\sigma}_{j+2})$  is the three-spin chirality operator [33, 34] and  $v$  is a dimensionless coupling constant. To detect the thermal signatures associated with HR, we couple the chain to a qubit subsystem (a two-level system) via the interaction term [35–37]:

$$H_I = \sum_{j=1}^N (g_1 \sigma_q^z + g_2 \sigma_q^x) \chi_j / 4, \quad (4)$$

where  $\sigma_q^{x,z}$  act on the qubit and  $g_{1,2}$  are coupling strengths. As shown in Fig. 1, coupling allows the qubit to exchange energy with the chain, inducing decoherence that serves as a proxy for the thermal bath of HR.

Diagonalization and Dynamics: A key feature of our setup is the existence of a conserved quantity associated with the qubit. The operator  $\mathcal{Q} \equiv g_1 \sigma_q^z + g_2 \sigma_q^x$  commutes with the total Hamiltonian,  $[\mathcal{Q}, H(t)] = 0$ . Consequently, the dynamics can be decomposed into independent sectors labeled by the eigenstates of  $\mathcal{Q}$ , denoted as  $|I_\pm\rangle$ :

$$|I_\pm\rangle = \frac{1}{\sqrt{1 + |\mathcal{G}_\pm|^2}} \begin{bmatrix} \mathcal{G}_\pm \\ 1 \end{bmatrix}, \quad \mathcal{G}_\pm = \frac{g_1 \pm \sqrt{g_1^2 + g_2^2}}{g_2}. \quad (5)$$

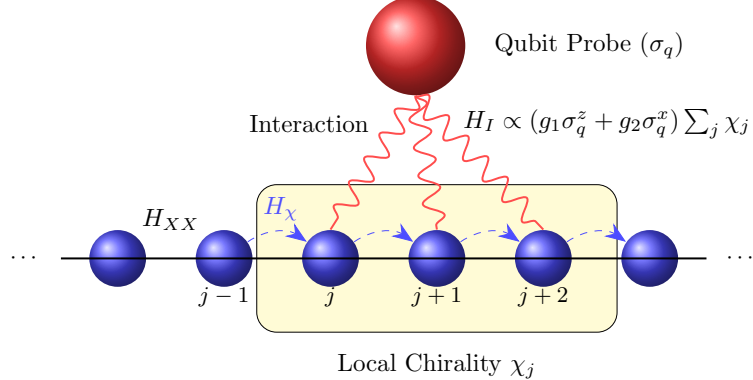


FIG. 1: Schematic diagram of the Qubit-Environment Coupling in Chiral Spin Chain.

In each sector corresponding to eigenvalues  $\pm\sqrt{g_1^2 + g_2^2}$ , the spin chain evolves under an effective Hamiltonian. Following the standard Jordan-Wigner and Fourier transformations [1, 38], the total Hamiltonian is diagonalized in momentum space (where  $p \in [-\pi, \pi]$ ):

$$H(t) = \sum_p E_{\pm}(p) c_p^\dagger c_p, \quad (6)$$

with the dispersion relation

$$E_{\pm}(p) = -2\mathcal{U} \cos(p) + V_e^{\pm} \sin(2p). \quad (7)$$

Here, the effective chiral coupling is modified by the probe interaction:  $V_e^{\pm} = v \pm \sqrt{g_1^2 + g_2^2}$ .

Quantum Phase Transition and Time Evolution: Analysis of the ground-state energy density reveals a Quantum Phase Transition (QPT) driven by the competition between the nearest-neighbor hopping and the chiral interaction. A discontinuity in the second derivative of the energy density occurs at the critical point  $|V_e^{\pm}| = |\mathcal{U}|$ .

This critical threshold is central to our analogue model, marking the boundary between distinct topological phases that we identify with the horizon formation condition. The physical origin of this QPT can be understood by drawing a parallel to Bosonic systems with higher spatial derivatives, such as the  $z = 3$  model studied in Ref. [39]. There, it was shown that higher-order derivative terms — corresponding to extended lattice neighbors — can violate the area law of entanglement entropy and trigger a phase transition due to the accumulation of zero modes. Similarly, in our model, the chirality operator acts as a higher-order correction to the standard  $XX$  chain dynamics. While  $H_{XX}$  governs nearest-neighbor transport,  $H_\chi$  induces three-site correlations that effectively modify the dispersion relation's

topology. The critical point  $|V_e^\pm| = |\mathcal{U}|$  can be mapped to a Lifshitz-like transition where the Fermi surface topology changes [40–42], mimicking the causal disconnection of a horizon.

We assume the system is initially prepared in an uncorrelated product state at  $t = t_0$ :

$$|\Psi(0)\rangle = |\psi_q(0)\rangle \otimes |\psi_E(0)\rangle, \quad (8)$$

where  $|\psi_E(0)\rangle$  is the vacuum of the pre-quench Hamiltonian  $H_{XX}$ , and the qubit is in a superposition  $|\psi_q(0)\rangle = \sum_{\ell=-,+} c_\ell |I_\ell\rangle$ . Due to the block-diagonal structure of the interaction, the time evolution splits into two branches, resulting in the entangled state for  $t \geq t_0$ :

$$|\Psi(t)\rangle = \prod_p \left[ \sum_{\ell=-,+} c_\ell e^{-iE_\ell(p)t} |I_\ell\rangle \right] \otimes |\psi_E(0)\rangle. \quad (9)$$

This state encodes the *thermal response* of the qubit to the sudden formation of the chiral background. In the rest of this work, we analyze this as an analogue of HR in BH.

Analogue BH Geometry: To go about this, we take the continuum limit of the above spin-chain model. As shown in Ref. [1], the spin chain maps onto a Dirac fermion propagating in a  $(1+1)$ –dimensional geometry:

$$ie_a^\mu \gamma^a (\partial_\mu + W_\mu) \psi(x) = 0, \quad (10)$$

where  $\psi$  is rescaled by the tetrad determinant  $\sqrt{|e|}$ ,  $W_\mu$  is the spin connection, and  $\gamma^a$  are the chiral gamma matrices (see Appendix B).

The sudden quench protocol naturally partitions spacetime into two distinct causal regions separated by the collapse time  $t_0$ , as illustrated in the Penrose diagram (Fig. 2). This mirrors the transition from an “in” Minkowski region ( $t < t_0$ ) to an “out” BH region ( $t \geq t_0$ ). The effective background metric is given by:

$$ds^2 = \begin{cases} dt^2 - \frac{1}{\mathcal{U}^2(x)} dx^2, & t < t_0 \\ g(x) dt^2 - 2\sqrt{1-g(x)} \frac{dt dx}{\mathcal{U}(x)} - \frac{dx^2}{\mathcal{U}^2(x)}, & t \geq t_0 \end{cases}, \quad (11)$$

where  $g(x) = 1 - V_e^{\pm 2} / \mathcal{U}^2(x)$ . Notably, the post-quench metric ( $t \geq t_0$ ) corresponds to the Gullstrand-Painlevé coordinates of a spherically symmetric spacetime [43], confirming the emergence of a BH geometry.

To analyze BH, we employ null coordinates to track the mixing of positive and negative frequency modes. The “in” region is described by coordinates  $(t, \mathcal{X})$ , while the “out”

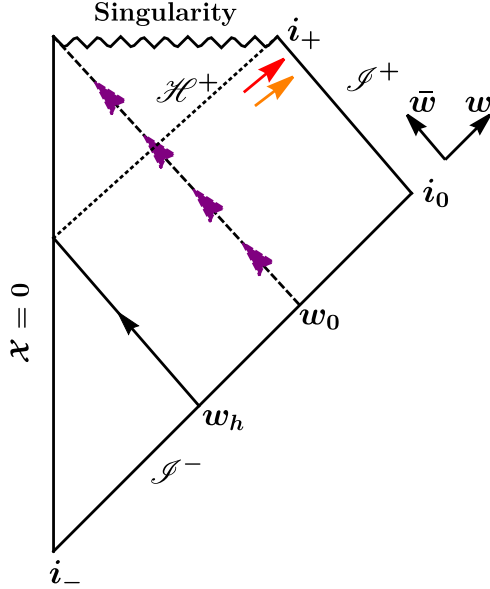


FIG. 2: Penrose diagram of the gravitational collapse process where a single shock wave located at  $w = w_0$  collapse to form a BH.

region utilizes  $(\tau, X)$ ; the explicit transformations are detailed in Table I. For the spatial inhomogeneity, we adopt the profile [1]:

$$\mathcal{U}(x) = \operatorname{sech}(x/\sigma)/\sqrt{2\sigma}, \quad (12)$$

where  $\sigma$  controls the width of the mass distribution. Horizon formation occurs when the "velocity" condition  $|V_e^\pm| = |\mathcal{U}|$  is met. For widths below a critical value  $\sigma_c \equiv 1/(2V_e^\pm)^2$ , this condition yields two symmetric horizons at:

$$x_{c\pm} = \pm\sigma \cosh^{-1} \left( \sqrt{\sigma_c/\sigma} \right). \quad (13)$$

This double-horizon structure bears a striking resemblance to the Reissner-Nordström geometry, where the interplay of mass and charge similarly generates inner and outer horizons. Finally, to analyze the radiation, we employ two complementary probe states:

**Plane Waves:** These allow for analytic tractability and explicitly demonstrate the thermal nature of the spectrum (thermality).

**Gaussian Wave Packets:** These localized states mimic realistic physical detectors, allowing us to track the propagation of Hawking quanta away from the horizon (detectability).

Region	Null Coordinates
“in”	$w_{\text{in}} = t + \mathcal{X}, \quad \bar{w}_{\text{in}} = t - \mathcal{X},$ $\mathcal{X} = \sqrt{2} \sigma^{3/2} \sinh\left(\frac{x}{\sigma}\right).$
“out”	$w_{\text{out}} = \tau + X, \quad \bar{w}_{\text{out}} = \tau - X,$ $\tau = t - \int_{x_0}^x \frac{dy V_e^\pm}{U^2(y)g(y)},$ $X = \frac{i\sigma^2}{(V_e^\pm)^2 \mathcal{X}_h} \tan^{-1}\left(\frac{\mathcal{X}}{i\mathcal{X}_h}\right), \quad \mathcal{X}_h = \pm\sigma\sqrt{2(\sigma_c - \sigma)}.$

TABLE I: Comparison of “in” and “out” null coordinates used in the analogue HR analysis.

*Analogue HR for Plane wave states:* Fig. 2 summarizes the causal structure via the Penrose diagram. The shock wave transforms the flat “in” region (past null infinity  $\mathcal{I}^-$ ) into a BH geometry, forming an event horizon  $\mathcal{H}^+$ . Outgoing null rays originating near  $\mathcal{H}^+$  experience exponential redshift before reaching future null infinity  $\mathcal{I}^+$ .

Positive-frequency ( $f$ ) ingoing modes at  $\mathcal{I}^-$  follow the standard form  $\psi_f^{\text{in}} \sim (e^{-i\bar{w}_{\text{in}}f}, e^{-iw_{\text{in}}f})^T$ . Tracing the outgoing rays backward to the horizon reveals the characteristic logarithmic relation:

$$\bar{w}_{\text{out}} \sim \frac{\sigma}{\sqrt{2(\sigma - \sigma_c)}} \log\left(\frac{w_{\text{in}} - w_h}{w_{\text{in}} - w_h - 2\mathcal{X}_h}\right), \quad (14)$$

where  $\mathcal{X}_h = \pm\sigma\sqrt{2(\sigma_c - \sigma)}$ . This logarithmic redshift mixes positive and negative frequency modes. Computing the Bogoliubov coefficients  $\beta_{ff'}$  via the Dirac inner product on a Cauchy surface yields the particle spectrum at late times:

$$n_f^P = \int_0^\infty df' |\beta_{ff'}|^2 = \frac{1}{e^{f/T_H} + 1}, \quad T_H = \sqrt{\frac{\sigma_c - \sigma}{2\sigma^2\sigma_c^2\pi^2}}. \quad (15)$$

For  $\sigma < \sigma_c$ , the plane-wave analysis confirms a purely thermal Fermi-Dirac spectrum with temperature  $T_H$ .

*Analogue HR for Gaussian states:* To model realistic detection, we employ localized Gaussian wave packets. We superpose the asymptotic plane-wave solutions with Gaussian envelopes ( $\sim e^{-w^2} e^{-iw^f}$ ), ensuring the states are spatially localized. The ratio of the resulting

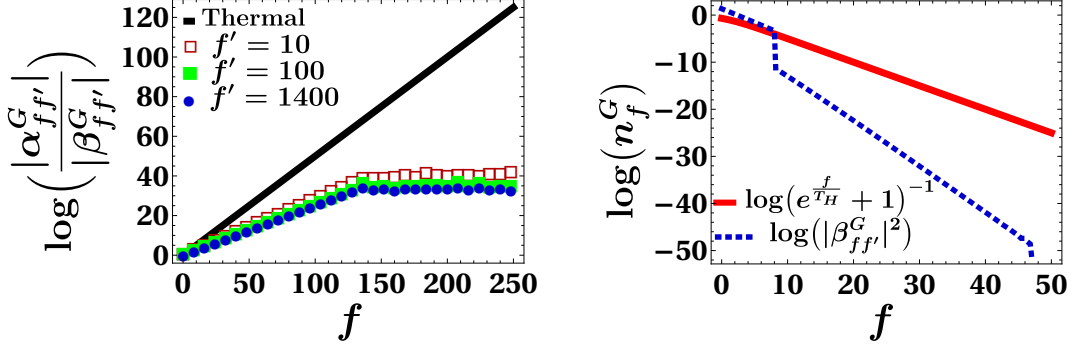


FIG. 3:  $\log \left( \left| \alpha_{ff'}^G \right| / \left| \beta_{ff'}^G \right| \right)$  as a function of outgoing frequency  $f$  for various fixed incoming frequencies  $f'$  (left), and particle number spectrum  $n_f^G$  as a function of  $f$  comparing the thermal prediction with the localized Gaussian wave-packet probe (right).

Bogoliubov coefficients is given by:

$$\frac{\alpha_{ff'}^G}{\beta_{ff'}^G} \sim e^{6i\omega_h f'} \frac{\mathcal{D}_{-\nu}(z^*/\sqrt{2})}{\mathcal{D}_{-\nu}(z/\sqrt{2})}, \quad (16)$$

where  $\mathcal{D}_{-\nu}$  is the Parabolic cylinder function,  $z = -2\omega_h - if'$ , and  $\nu = 1 + if/(2\pi T_H)$ . Unlike the delocalized plane-wave case, this ratio is generally non-thermal. This non-thermal behavior can be understood in terms of grey-body factors describing the fact that not all modes produced near the horizon reach the detector unchanged: part of the wave packet is reflected, scattered, or distorted by the background before detection [26, 27].

Figure 3 illustrates the effects of localization at fixed  $T_H = 2$  as determined from (15) with  $\sigma = 0.1014$  and  $\sigma_c = 0.1115$  is fixed by choosing  $v = 1$ ,  $g_1 = 1$ , and  $g_2 = 1/2$ . The left panel shows the logarithmic Bogoliubov ratio. At low frequencies, it follows the linear thermal scaling, but at high frequencies, it saturates to a constant. This indicates that physical detectors are insensitive to trans-Planckian modes. The right panel confirms that the particle number spectrum  $n_f^G$  deviates from the ideal thermal prediction [44]. Thus, strict thermality is a feature of idealized infinite-duration measurements; realistic probes observe deviations at high energies.

Finally, we examine the statistical nature of the radiation. Figure 4 displays the spectral distribution of outgoing modes for both probe types plotted against the Poisson parameter  $s = \langle n_f \rangle$ . Contrary to Wigner–Dyson statistics  $P_{WD} = (\pi s/2)e^{-\pi s^2/4}$  [45], both plane-wave and Gaussian distributions are well-described by the Poisson form  $e^{-s/s_0}$ . This demonstrates that the statistical character of HR is robust: even when localization effects modify the

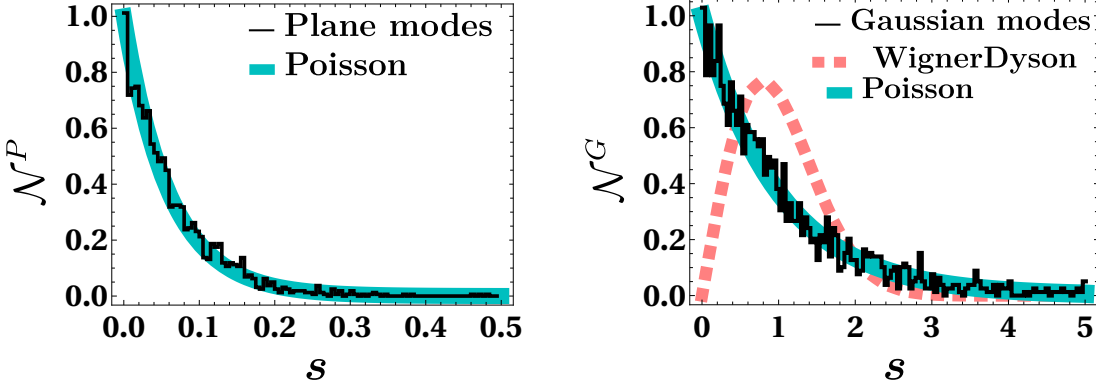


FIG. 4: Poissonian statistics of Hawking emission for the plane-wave (left) and Gaussian wave-packets (right).

spectrum, the emission process remains fundamentally Poissonian.

This is the key result of this work regarding which we want to discuss the underlying physical reason for the universal Poissonian behavior. HR originates from vacuum pair-production events which, in the absence of significant backreaction, are statistically independent and uncorrelated in time. This independence renders the emission a Poisson process, analogous to random tunneling events [4, 43]. Since Gaussian wave packets are formed by linear superpositions of plane waves without introducing phase coherence, they preserve this intrinsic stochasticity. Thus, the Poissonian statistics reflect the fundamental randomness of vacuum fluctuations, which is robust against the spatial localization of the probe.

*Qubit as a quantum probe:* To operationalize the detection of HR, we couple a stationary qubit to the spin chain, acting as an Unruh-DeWitt detector [46]. The qubit's relaxation and decoherence dynamics encode the correlation structure of the background field. The fidelity of this “thermometer” depends critically on the coupling strength, revealing two distinct physical regimes.

**Strong coupling regime ( $|g_2| > |\mathcal{U}|, |v|$ ):** We first consider the qubit strongly coupled to the chain. By tracing out the environment, we compute the exact reduced density matrix  $\rho_q(t)$  (see Appendix C for details). In this regime, the spin chain acts as a finite many-body reservoir. The interaction induces energy exchange, causing the qubit populations to relax to a steady state on a timescale  $\tau_0 \propto (g_1^2 + g_2^2)^{-1/2}$  leading to rapid decoherence<sup>1</sup>.

<sup>1</sup>The decoherence function, defined as  $D(t) = \prod_p |P_{qe}(p, t)|^2$ , quantifies the magnitude of coherence present in the reduced density matrix.

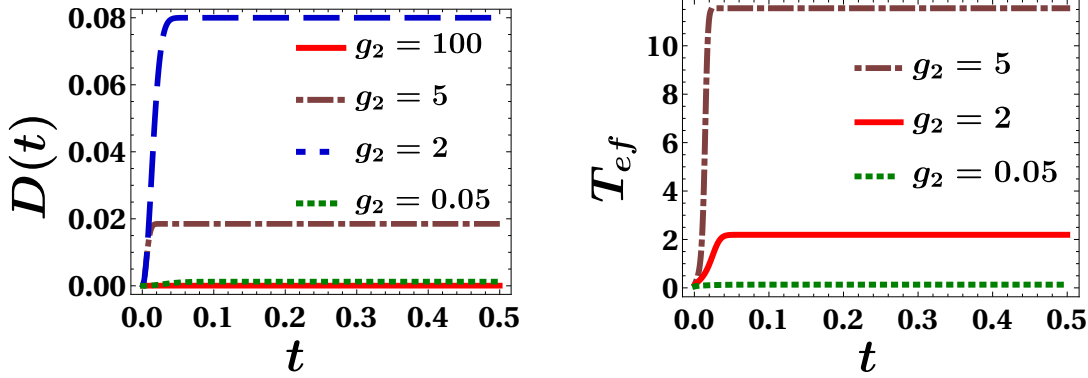


FIG. 5: The dynamics of the decoherence factor (left) and the effective temperature (right) of the qubit for different values of  $g_2$ .

As shown in Fig. 5,  $D(t)$  decays sharply as the coupling between qubit and environment becomes stronger. However, the effective temperature  $T_{ef}$  extracted from the steady-state populations does not coincide with the Hawking temperature  $T_H$ . Instead,  $T_{ef}$  depends non-trivially on the coupling parameters  $g_{1,2}$  and the global properties of the chain. In this strong-coupling limit, the qubit effectively thermalizes with the entire spin-chain environment rather than selectively probing the horizon-induced modes. Consequently, a strongly coupled qubit is not a faithful probe of HR.

**Weak coupling regime ( $|g_2| \ll |\mathcal{U}|, |v|$ ):** In this limit, the spin chain acts as a Markovian thermal bath. The reduced qubit dynamics are governed by rate equations determined solely by the bath spectral density  $J(\omega)$  and the mode occupation [47]:

$$\dot{\rho}_{ee} = -\Gamma_{\downarrow}\rho_{ee} + \Gamma_{\uparrow}\rho_{gg}, \quad (17)$$

where the rates  $\Gamma_{\uparrow,\downarrow} \propto J(\omega)(e^{\pm\omega/T_H} + 1)^{-1}$  follow the Fermi-Dirac distribution. Unlike the strong coupling case, here the qubit is insensitive to microscopic details and probes only the thermal state of the Fermionic field. Solving the master equation confirms that the qubit relaxes to a stationary state  $\rho_{ee}^s = (e^{\omega/T_H} + 1)^{-1}$ . Figure 6 illustrates the equilibration of the population ratio  $\log(\rho_{ee}/\rho_{gg})$ . The slope of this ratio in the steady state directly yields the Hawking temperature  $T_H$ . Thus, in the weak-coupling limit, the qubit functions as a faithful quantum thermometer, allowing for the experimental determination of the analogue Hawking temperature via simple population tomography.

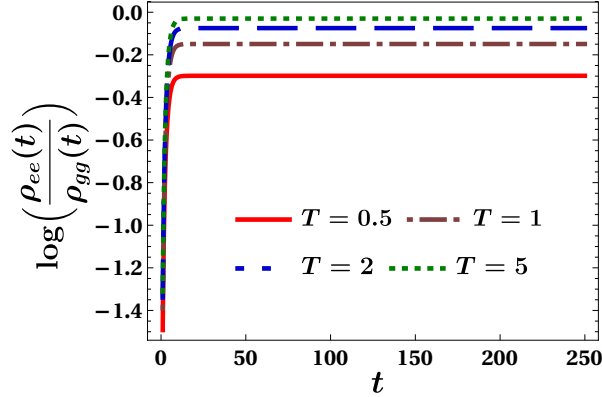


FIG. 6: Time evolution of the logarithmic qubit population ratio for different values of the environmental temperature  $T$  showing saturation at long times.

*Conclusions and Outlook:* In this work, we have established a robust analogue of HR in a chiral spin chain modeled as a sudden quantum quench. By deriving the response of both field-theoretic modes and quantum sensor probes, we have clarified the interplay between horizon formation, thermality, and the detectability.

First, our analysis distinguishes between mathematical thermality and physical detectability. While idealized plane-wave modes recover a strictly thermal spectrum, we demonstrate that physically realistic probes — modeled as localized Gaussian wave packets — exhibit deviations from the Planckian distribution. These deviations arise from the finite localization of the detector, which imposes a frequency-dependent filtering analogous to greybody factors in gravitational systems. This result challenges the conventional view of HR as a structureless, information-free thermal bath; instead, it suggests that physical measurement processes naturally imprint non-thermal features onto the observed spectrum, potentially encoding information about the detector-horizon interplay at finite scales.

Second, the universal nature of our results sheds light on the role of formation history. In our previous work, we showed that the geometric satisfaction of the Hoop conjecture is a necessary but insufficient condition for horizon formation in the percolation picture [1, 48]. However, the present analysis reveals that the stationary HR is insensitive to these formation criteria. The emission statistics remain robustly Poissonian for both plane-wave and Gaussian probes. This insensitivity is not a limitation of the model but a manifestation of the universal kinematics of the near-horizon region. The radiation effectively *washes out* the memory of the formation scale (Hoop information), reinforcing the idea that HR acts as

a late-time attractor that is independent of the microscopic details of the collapse.

Third, we emphasize that our model operates strictly within the continuum limit of the spin chain. Consequently, it reproduces the continuous Hawking spectrum characteristic of semiclassical gravity but remains blind to discrete lattice effects such as the Bekenstein-Mukhanov spectrum [49]. The quantization of horizon area, which implies a discrete line spectrum for radiation, requires retaining the discrete lattice structure of the chain or use other probes like in fluid-gravity correspondence [50].

Finally, we have identified the operational conditions required to measure this effect in a quantum simulation. We showed that a qubit acts as a faithful thermometer only in the weak-coupling regime, where it essentially probes the spectral density of the bath. In contrast, strong coupling induces complex many-body entanglements where the qubit thermalizes with the entire environment rather than the horizon specifically. This distinction is critical for future experimental realizations of analogue gravity in quantum spin systems, providing a clear protocol for distinguishing genuine Hawking temperatures from spurious environmental heating, especially in setups that mimic cosmological expansion [51].

**Acknowledgments:** The authors thank Soumya Bhattacharya, Indranil Chakraborty, Māhesh Chandran, K. Hari, P. George Christopher, Tausif Parvez, Tapobrata Sarkar, and Archit Vidyarthi for discussions and comments on the earlier draft. The work is supported by SERB-CRG/2022/002348.

## Appendix A: The Model and its Diagonalization

The total time-dependent Hamiltonian  $H(t)$  is composed of three parts: the conventional XX spin-chain Hamiltonian, a chirality operator term, and an interaction term describing the coupling between the qubit and the chiral sector:

$$H(t) = - \sum_{j=1}^N \frac{\mathcal{U}}{2} (\sigma_j^x \sigma_{j+1}^x + \sigma_j^y \sigma_{j+1}^y) + \Theta(t - t_0) \sum_{j=1}^N \left[ \frac{v}{4} \chi_j + (g_1 \sigma_q^z + g_2 \sigma_q^x) \frac{\chi_j}{4} \right]. \quad (\text{A1})$$

Here,  $\chi_j = \vec{\sigma}_j \cdot (\vec{\sigma}_{j+1} \times \vec{\sigma}_{j+2})$  denotes the three-spin chirality operator,  $v$  is a dimensionless coupling constant,  $\sigma_q^{x,z}$  are the Pauli matrices acting on the qubit, and  $g_{1,2}$  represent the corresponding coupling strengths.

To diagonalize the Hamiltonian, we first observe that the operator  $\mathcal{Q} \equiv g_1 \sigma_q^z + g_2 \sigma_q^x$  commutes with the total Hamiltonian,  $[\mathcal{Q}, H(t)] = 0$ . As a result,  $\mathcal{Q}$  is a conserved quantity

and can be treated as a constant within each sector. Its eigenvalues are  $\pm\sqrt{g_1^2 + g_2^2}$ , with corresponding eigenstates given by [35, 36]:

$$|I_{\pm}\rangle = \frac{1}{\sqrt{1 + |\mathcal{G}_{\pm}|^2}} \begin{bmatrix} \mathcal{G}_{\pm} \\ 1 \end{bmatrix}, \quad \mathcal{G}_{\pm} = \frac{g_1 \pm \sqrt{g_1^2 + g_2^2}}{g_2}. \quad (\text{A2})$$

This allows us to replace the qubit subsystem by its spectral decomposition:

$$g_1\sigma_q^z + g_2\sigma_q^x \equiv \sum_{\ell=\pm} \ell\sqrt{g_1^2 + g_2^2} |I_{\ell}\rangle \langle I_{\ell}|, \quad (\text{A3})$$

where  $|I_{\ell}\rangle$  denote the corresponding qubit eigenstates. As a consequence, the full Hamiltonian decomposes into two independent sectors labeled by  $\ell = \pm$ . The diagonalization of the remaining Hamiltonian—comprising the standard XX spin chain and the three-spin chirality term—has been carried out in detail in Ref. [1] using the Jordan–Wigner transformation followed by a Fourier transformation. The resulting single-particle dispersion relation is given by  $E(p) = -2\mathcal{U}\cos(p) + v\sin(2p)$ . Incorporating the contribution from the qubit sector, the total Hamiltonian can therefore be written in diagonal form as

$$H(t) = \sum_p E_{\pm}(p) c_p^{\dagger} c_p, \quad E_{\pm}(p) = -2\mathcal{U}\cos(p) + V_e^{\pm} \sin(2p), \quad (\text{A4})$$

where  $V_e^{\pm} = v \pm \sqrt{g_1^2 + g_2^2}$ . Here  $p \in [-\pi, \pi]$  denotes the lattice quasi-momentum,  $E_{\pm}(p)$  is the dispersion relation for the total Hamiltonian, and  $c_p$  ( $c_p^{\dagger}$ ) are fermionic annihilation (creation) operators obtained via Fourier transformation.

## Appendix B: Analog Hawking Radiation

### 1. Plane Wave States

The covariant Dirac equation for massless spinor fields in curved spacetime is given by [1]:

$$ie_a^{\mu} \gamma^a (\partial_{\mu} + W_{\mu}) \psi(x) = 0, \quad (\text{B1})$$

where  $W_{\mu}$  denotes the spin connection, and  $\gamma^a$  are the Dirac gamma matrices. In the Dirac representation, these are chosen as

$$\gamma^0 = \begin{pmatrix} 1 & 0 \\ 0 & -1 \end{pmatrix}, \quad \gamma^1 = \begin{pmatrix} 0 & -i \\ -i & 0 \end{pmatrix}. \quad (\text{B2})$$

The gamma matrices obey the anti-commutation relation  $\{\gamma^a, \gamma^b\} = 2\eta^{ab}$  with the Minkowski metric  $\eta^{ab} = \text{diag}(1, -1, -1, -1)$ . To solve Eq. (B1), it is convenient to work in the chiral representation, in which the left and right-moving modes decouple. The gamma matrices in the chiral basis are obtained via the unitary transformation  $S$ :  $\gamma_c^\mu = S^{-1}\gamma^\mu S$  yielding

$$\gamma_c^0 = \begin{pmatrix} 0 & 1 \\ 1 & 0 \end{pmatrix}, \quad \gamma_c^1 = \begin{pmatrix} 0 & -1 \\ 1 & 0 \end{pmatrix}, \quad \text{with} \quad S = \frac{1}{\sqrt{2}} \begin{pmatrix} 1 & 1 \\ i & -i \end{pmatrix}. \quad (\text{B3})$$

In the flat spacetime “in” region, it is natural to introduce coordinates  $(t, \mathcal{X})$  with the spatial coordinate defined through  $d\mathcal{X} = dx/\mathcal{U}(x)$ . In these coordinates, the Dirac equation and its plane wave solution are

$$i(\gamma_c^0 \partial_t + \gamma_c^1 \partial_{\mathcal{X}}) \psi_f^{\text{in}}(t, \mathcal{X}) = 0, \quad \psi_f^{\text{in}}(t, \mathcal{X}) \sim \begin{pmatrix} e^{-i\bar{w}_{\text{in}} f} \\ e^{-i w_{\text{in}} f} \end{pmatrix}, \quad (\text{B4})$$

for positive frequency ingoing modes with the ingoing null coordinates  $w_{\text{in}} = t + \mathcal{X}$ ,  $\bar{w}_{\text{in}} = t - \mathcal{X}$ . In contrast, the “out” region corresponds to a curved spacetime and is described by coordinates  $(\tau, X)$ . The Dirac equation and its plane wave solution in the “out” region are

$$i(\gamma_c^\tau \partial_\tau + \gamma_c^X \partial_X + \gamma_c^X W_\tau + \gamma_c^\tau W_X) \psi_f^{\text{out}}(\tau, X) = 0, \quad \psi_f^{\text{out}}(\tau, X) \sim \begin{pmatrix} e^{-i\bar{w}_{\text{out}} f} \\ e^{-i w_{\text{out}} f} \end{pmatrix}, \quad (\text{B5})$$

for positive frequency outgoing modes with the outgoing null coordinates  $w_{\text{out}} = \tau + X$ ,  $\bar{w}_{\text{out}} = \tau - X$ . The explicit coordinate transformations take the forms

$$\tau = t - \int_{x_0}^x \frac{dy V_e^\pm}{\mathcal{U}^2(y) g(y)}, \quad X = \frac{i\sigma^2}{(V_e^\pm)^2 \mathcal{X}_h} \tan^{-1} \left( \frac{\mathcal{X}}{i\mathcal{X}_h} \right), \quad \mathcal{X}_h = \pm\sigma\sqrt{2(\sigma_c - \sigma)}. \quad (\text{B6})$$

In these coordinates, the curved-spacetime gamma matrices in the chiral representation are

$$\gamma_c^\tau = \frac{1}{g(X)} \begin{pmatrix} 0 & 1 + \frac{V_e^\pm}{\mathcal{U}(X)} \\ 1 - \frac{V_e^\pm}{\mathcal{U}(X)} & 0 \end{pmatrix}, \quad \gamma_c^X = \frac{1}{g(X)} \begin{pmatrix} 0 & -1 - \frac{V_e^\pm}{\mathcal{U}(X)} \\ 1 - \frac{V_e^\pm}{\mathcal{U}(X)} & 0 \end{pmatrix}, \quad (\text{B7})$$

and the corresponding spin-connection components entering the Dirac equation are

$$W_\tau = \frac{(V_e^\pm)^2 \mathcal{U}'(X)}{2\mathcal{U}^3(X) g(X)} \gamma^0, \quad W_X = \frac{V_e^\pm \mathcal{U}'(X)}{2\mathcal{U}^2(X) g(X)} \gamma^0, \\ \mathcal{U}(X) = \frac{1}{\sqrt{2\sigma}} \left[ 1 + \left( 1 - \frac{1}{2\sigma V_e^{\pm 2}} \right) \cot^2 \left( \frac{X V_e^\pm \sqrt{2\sigma V_e^{\pm 2} - 1}}{\sigma} \right) \right]^{-1/2}. \quad (\text{B8})$$

The calculation of Hawking radiation crucially relies on tracing outgoing field modes backward in time toward the horizon. The above null coordinates play a central role in tracing

outgoing modes backward toward the horizon and in evaluating the Bogoliubov coefficients responsible for Hawking radiation. As emphasized in Ford's review [52], this backward propagation reveals the exponential redshift experienced by outgoing rays near the horizon:

$$\bar{w}_{\text{out}} \sim \frac{\sigma}{\sqrt{2(\sigma - \sigma_c)}} \log \left( \frac{w_{\text{in}} - w_h}{w_{\text{in}} - w_h - 2\mathcal{X}_h} \right) , \quad (\text{B9})$$

which in turn governs the nontrivial Bogoliubov mixing between positive and negative-frequency modes. The Bogoliubov coefficient  $\beta_{ff'}$  is defined by the Dirac inner product between the “in” and “out” modes is

$$\beta_{ff'} \equiv (\psi_f^{\text{out}}, \psi_{f'}^{\text{in}})_D = \int_{\Sigma} d\Sigma_{\mu} \bar{\psi}_f^{\text{out}} \gamma^{\mu} \psi_{f'}^{\text{in}} , \quad (\text{B10})$$

where  $d\Sigma_{\mu} = n_{\mu} d\Sigma$  is the directed surface element, and  $n_{\mu}$  is the unit normal to the Cauchy surface  $\Sigma$ . The above integral is dominated by contributions from the vicinity of the horizon,

$$\beta_{ff'} \sim \int_{-\infty}^{w_h} dw_{\text{in}} e^{iw_{\text{out}}f} e^{-iw_{\text{in}}f'} = -e^{-iw_hf'} (if')^{-1 - \frac{if}{2\pi T_H}} \Gamma \left( 1 + \frac{if}{2\pi T_H} \right) , \quad (\text{B11})$$

with  $T_H = \sqrt{\frac{\sigma_c - \sigma}{2\sigma^2\sigma_c^2\pi^2}}$  is the Hawking temperature and  $n_{\mu} = (1, 0)$  for a surface with constant  $\bar{w}$ . Similarly one can also obtain the other Bogoliubov coefficient,  $|\alpha_{ff'}| = e^{f/2T_H} |\beta_{ff'}|$ . Then, using the normalization condition  $\int_0^{\infty} df' (|\alpha_{ff'}|^2 + |\beta_{ff'}|^2) = 1$ , we obtain the particle spectrum at late times as

$$n_f^P = \int_0^{\infty} df' |\beta_{ff'}|^2 = \frac{1}{e^{f/T_H} + 1} . \quad (\text{B12})$$

## 2. Gaussian Wave Packets

Having established the plane-wave solutions of the Dirac equation in the “in” and “out” regions, we now construct localized Gaussian wave packet solutions. These are defined for the “in” and “out” regions respectively as

$$\psi_{f,G}^{\text{in}} \sim \begin{pmatrix} e^{-\bar{w}_{\text{in}}^2} e^{-i\bar{w}_{\text{in}}f} \\ e^{-w_{\text{in}}^2} e^{-iw_{\text{in}}f} \end{pmatrix} , \quad \psi_{f,G}^{\text{out}} \sim \begin{pmatrix} e^{-\bar{w}_{\text{out}}^2} e^{-i\bar{w}_{\text{out}}f} \\ e^{-w_{\text{out}}^2} e^{-iw_{\text{out}}f} \end{pmatrix} , \quad (\text{B13})$$

for positive frequency modes, where the subscript  $G$  stands for Gaussian. Since these Gaussian wave packets are constructed in analogy with the plane-wave modes, the Bogoliubov

transformation relating ingoing and outgoing solutions proceeds in complete analogy with the plane-wave case. Consequently, the Bogoliubov coefficients are

$$\begin{aligned}\beta_{ff'}^G &\sim \int_{-\infty}^{w_h} dw_{\text{in}} e^{iw_{\text{out}}f} e^{-iw_{\text{in}}f'} e^{-w_{\text{out}}^2 - w_{\text{in}}^2} \\ &= (-1)^{\nu+1} e^{-iw_h f'} e^{-w_h^2} \Gamma(\nu) 2^{-\frac{\nu}{2}} e^{\frac{z^2}{8}} \mathcal{D}_{-\nu} \left( \frac{z}{\sqrt{2}} \right),\end{aligned}\quad (\text{B14})$$

and

$$\begin{aligned}\alpha_{ff'}^G &\sim \int_{-\infty}^{w_h} dw_{\text{in}} e^{iw_{\text{out}}f} e^{iw_{\text{in}}f'} e^{-w_{\text{out}}^2 - w_{\text{in}}^2} \\ &= (-1)^{\nu+1} e^{iw_h f'} e^{-w_h^2} \Gamma(\nu) 2^{-\frac{\nu}{2}} e^{\frac{z^*2}{8}} \mathcal{D}_{-\nu} \left( \frac{z^*}{\sqrt{2}} \right),\end{aligned}\quad (\text{B15})$$

where  $\mathcal{D}_{-\nu}$  is the Parabolic cylinder function,  $z = -2w_h - if'$ , and  $\nu = 1 + if/(2\pi T_H)$ . Then, the ratio of Bogoliubov coefficients for Gaussian wave packets can be evaluated as

$$\frac{\alpha_{ff'}^G}{\beta_{ff'}^G} \sim e^{6iw_h f'} \frac{\mathcal{D}_{-\nu}(z^*/\sqrt{2})}{\mathcal{D}_{-\nu}(z/\sqrt{2})}. \quad (\text{B16})$$

This ratio is, in general, non-thermal. This deviation from perfect thermality can be attributed to grey-body factors [26, 27], which encode the fact that modes generated near the horizon do not propagate to the detector without modification. As they travel through the background geometry, portions of the wave packet are partially reflected, scattered, or otherwise distorted, leading to a frequency-dependent filtering of the detected spectrum. Furthermore, for low-frequency outgoing modes ( $f \simeq 0$ ), the ratio reduces to  $\frac{\alpha_{ff'}^G}{\beta_{ff'}^G} \approx 1$ , indicating an equal contribution from positive and negative-frequency components. As a consequence, the particle occupation number is given by

$$n_f^G = \int_0^\infty df' |\beta_{ff'}|^2 = \frac{1}{2}, \quad (\text{B17})$$

which corresponds to the standard Fermi level.

## Appendix C: Qubit Dynamics and Decoherence

### 1. Exact Dynamics in Strong Coupling

For the general coupling case, the reduced density matrix of the qubit  $\rho_q(t) = \text{Tr}_E [ |\Psi(t)\rangle \langle \Psi(t)| ]$  is obtained by tracing over the spin-chain modes  $E$ . The matrix elements in the basis

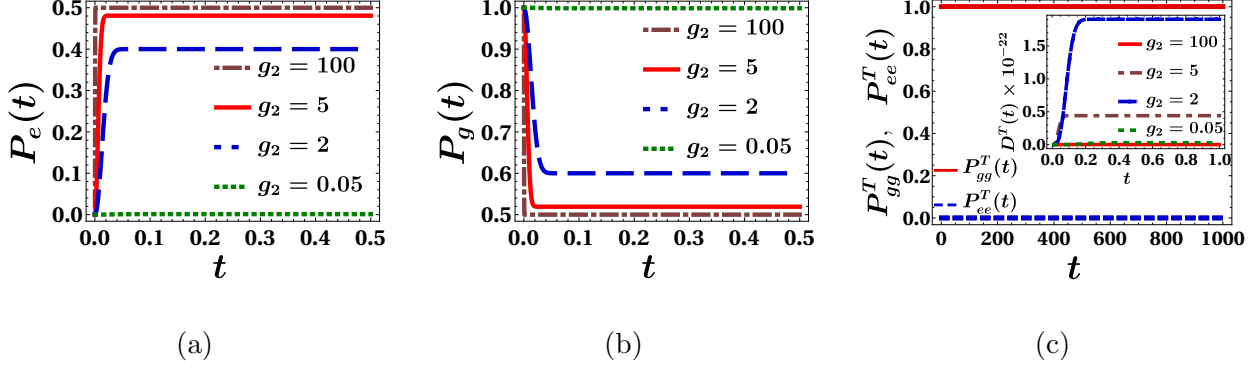


FIG. 7: Time evolution of the qubit populations for different values of the coupling strength  $g_2$ , with  $g_1 = 1$  fixed. **(a)** Excited-state and **(b)** ground-state populations when the spin chain is initialized in its ground state. **(c)** Freezing of the qubit populations when the spin chain is prepared in a thermal state, signaling the suppression of coherent population transfer. The inset in (c) displays the corresponding decoherence factor induced by the thermal spin-chain environment.

$\{|g\rangle, |e\rangle\}$  are given by:

$$\begin{aligned} P_{gg}(p, t) &= \frac{2g_1^2 + g_2^2 (\cos(\Omega_R t) + 1)}{2(g_1^2 + g_2^2)}, \\ P_{eg}(p, t) &= \frac{g_1 g_2 (\cos(\Omega_R t) - 1)}{2(g_1^2 + g_2^2)} - i \frac{g_2 \sin(\Omega_R t)}{2\sqrt{g_1^2 + g_2^2}}, \end{aligned} \quad (C1)$$

where  $P_{ee}(p, t) = 1 - P_{gg}(p, t)$  and  $P_{ge}(p, t) = P_{eg}^*(p, t)$ . The Rabi frequency is defined as  $\Omega_R = 2\sqrt{g_1^2 + g_2^2} \sin 2p$ . The total population is the product over all quasi-momenta  $p$ . The decoherence function [36], defined as  $D(t) = \prod_p |P_{ge}(p, t)|^2$ , quantifies the magnitude of coherence present in the reduced density matrix. We emphasize that since the qubit starts in an energy eigenstate ( $D(0) = 0$  by construction),  $D(t)$  measures the suppression of *dynamically generated* coherence. As the qubit-chiral interaction is switched on,  $D(t)$  initially increases, indicating the buildup of coherence. At later times, however, it saturates, reflecting the qubit completely entangled with the environmental degrees of freedom. This definition differs from commonly used decoherence measures, where  $D(t) = 1$  corresponds to a pure, fully coherent state and  $D(t) = 0$  signals complete loss of coherence.

The left and middle panels of Fig. 7 show the time evolution of the qubit populations with the system initialized in the ground state ( $P_{gg}(0) = 1$ ). Although the combined system evolves unitarily, the spin chain acts as a finite many-body reservoir with internal excitations

and correlations. Consequently, both phase and energy information of the qubit are rapidly redistributed into the spin-chain degrees of freedom via entanglement.

Due to this rapid decoherence and energy exchange, the qubit populations relax to steady-state values on a short timescale  $\tau_0 = \sqrt{N^{-1} \log(\epsilon^{-1})/(g_1^2 + g_2^2)}$  (for accuracy  $\epsilon = 10^{-4}$ ). Beyond this timescale, the steady state can be characterized by an effective temperature:

$$T_{\text{ef}} = \frac{|\mathcal{U} - v|}{\log(P_g^s/P_e^s)}, \quad (\text{C2})$$

where  $P_g^s$  and  $P_e^s$  denote the steady-state ground and excited populations, respectively, and  $|\mathcal{U} - v|$  is the energy exchange scale.

We have explicitly verified that this effective temperature remains distinct from the Hawking temperature  $T_H$ , even when the spin chain is initialized in a thermal state  $\rho_E \propto e^{-H_E/T}$ . For such thermally disordered configurations, the qubit population dynamics are given by:

$$\begin{aligned} P_{gg}^T(t) &= \prod_p \left[ 1 - \frac{g_2^2 f_p (1 - \cos(\Omega_R t))}{2(g_1^2 + g_2^2)} \right], \quad f_p = \frac{1}{e^{\frac{E(p)}{T}} + 1}, \\ P_{eg}^T(t) &= \prod_p f_p \left[ \frac{g_1 g_2}{2(g_1^2 + g_2^2)} (-1 + \cos(\Omega_R t)) - i \frac{g_2 \sin(\Omega_R t)}{2\sqrt{g_1^2 + g_2^2}} \right]. \end{aligned} \quad (\text{C3})$$

In this thermal regime, the qubit populations remain effectively frozen ( $P_{gg}^T(t) \approx 1$ ), as shown in Fig. 7(c). The corresponding decoherence function  $D^T(t)$  exhibits negligible decay (Fig. 7(c) inset). This prevents meaningful temperature extraction, confirming that strong coupling is unsuitable for probing  $T_H$ .

## 2. Weak Coupling Rates

In the weak-coupling regime ( $|g_2| \ll |\mathcal{U}|, |v|$ ), the qubit dynamics are governed by the Dirac spectrum of the chiral spin chain, which acts as an effective thermal reservoir. The reduced dynamics are described by the Born–Markov approximation, leading to rate equations determined entirely by the spectral properties of the environment. The relevant bath spectral density is defined as:

$$J(\omega) = 2\pi (g_1^2 + g_2^2) \varrho(\omega), \quad \varrho(\omega) = \frac{1}{2\pi} \sum_{E(p)=\omega} \frac{1}{|\partial_p E(p)|}, \quad (\text{C4})$$

where  $\omega$  denotes the energy exchange and  $\varrho(\omega)$  is the density of states. For the dispersion relation considered here, this simplifies to  $J(\omega) = (g_1^2 + g_2^2)/|2(\mathcal{U} - v)|$ . The transition rates

are:

$$\Gamma_{\uparrow} = J(\omega)f_D(\omega), \quad \Gamma_{\downarrow} = J(\omega)(1 - f_D(\omega)), \quad (C5)$$

where  $f_D(\omega) = (e^{\omega/T} + 1)^{-1}$ . These rates yield the population dynamics:

$$\dot{\rho}_{ee} = -\Gamma_{\downarrow}\rho_{ee} + \Gamma_{\uparrow}(1 - \rho_{ee}) \implies \rho_{ee}(t) = f_D(\omega) (1 - e^{-J(\omega)t}). \quad (C6)$$

The ground-state population  $\rho_{gg}(t) = 1 - \rho_{ee}(t)$  relaxes toward a stationary thermal state. This satisfies the detailed balance condition  $\Gamma_{\uparrow}/\Gamma_{\downarrow} = e^{-\omega/T_H}$ , validating the thermalization observed in Fig. 6 of the main text.

At the horizon ( $|\mathcal{U}| = v$ ), the bath spectral density diverges ( $J(\omega) \rightarrow \infty$ ), signaling infinitely strong mode coupling. In this limit, the qubit states are fully governed by the Dirac thermal spectrum. Thus, as long as the analog black hole exists, the detector couples to the Dirac spectrum rather than the vacuum, allowing  $T_H$  to be extracted as an emergent property of the environment.

---

[1] Nitesh Jaiswal and S. Shankaranarayanan, “Analog charged black hole formation via percolation: Exploring cosmic censorship and hoop conjecture,” *Phys. Rev. D* **111**, L101502 (2025).

[2] L. Parker, “Probability Distribution of Particles Created by a Black Hole,” *Phys. Rev. D* **12**, 1519–1525 (1975).

[3] Steven Corley and Ted Jacobson, “Hawking spectrum and high frequency dispersion,” *Phys. Rev. D* **54**, 1568–1586 (1996).

[4] S. Shankaranarayanan, T. Padmanabhan, and K. Srinivasan, “Hawking radiation in different coordinate settings: Complex paths approach,” *Class. Quant. Grav.* **19**, 2671–2688 (2002), [arXiv:gr-qc/0010042](https://arxiv.org/abs/gr-qc/0010042).

[5] S. Shankaranarayanan, K. Srinivasan, and T. Padmanabhan, “Method of complex paths and general covariance of Hawking radiation,” *Mod. Phys. Lett. A* **16**, 571–578 (2001), [arXiv:gr-qc/0007022](https://arxiv.org/abs/gr-qc/0007022).

[6] Roberto Casadio, “On dispersion relations and the statistical mechanics of Hawking radiation,” *Class. Quant. Grav.* **19**, 2453–2462 (2002), [arXiv:hep-th/0111287](https://arxiv.org/abs/hep-th/0111287).

[7] S. Santhosh Kumar and S. Shankaranarayanan, “Quantum entanglement and Hawking temperature,” *Eur. Phys. J. C* **76**, 400 (2016), [arXiv:1504.00501 \[quant-ph\]](https://arxiv.org/abs/1504.00501).

[8] Kunal Pal, Kuntal Pal, and Tapobrata Sarkar, “Analogue Metric in a Black-Bounce Background,” *Universe* **8**, 197 (2022), arXiv:2204.06395 [gr-qc].

[9] Matteo Smerlak and Suprit Singh, “New perspectives on hawking radiation,” *Phys. Rev. D* **88**, 104023 (2013).

[10] Kunal Pal and Uwe R. Fischer, “Quantum nonlinear effects in the number-conserving analog gravity of Bose-Einstein condensates,” *Phys. Rev. D* **110**, 116022 (2024), arXiv:2410.13596 [gr-qc].

[11] Susobhan Mandal and S. Shankaranarayanan, “Modified gravity theories at different curvature scales,” in *Encyclopedia of Astrophysics (First Edition)*, edited by Ilya Mandel (Elsevier, Oxford, 2026) first edition ed., pp. 73–111, arXiv:2502.07437 [gr-qc].

[12] K. S. Virbhadra, “Distortions of images of Schwarzschild lensing,” *Phys. Rev. D* **106**, 064038 (2022), arXiv:2204.01879 [gr-qc].

[13] Carlos Barcelo, Stefano Liberati, and Matt Visser, “Analogue gravity,” *Living Rev. Rel.* **8**, 12 (2005), arXiv:gr-qc/0505065.

[14] Jeff Steinhauer, “Observation of self-amplifying Hawking radiation in an analog black hole laser,” *Nature Phys.* **10**, 864 (2014), arXiv:1409.6550 [cond-mat.quant-gas].

[15] Jeff Steinhauer and Juan Ramón Muñoz de Nova, “Self-amplifying Hawking radiation and its background: a numerical study,” *Phys. Rev. A* **95**, 033604 (2017), arXiv:1608.02544 [cond-mat.quant-gas].

[16] Pritam Banerjee, Suvankar Paul, and Tapobrata Sarkar, “Curvature couplings of massless fermions in analog gravity,” *Phys. Lett. B* **789**, 160–166 (2019).

[17] Chunyu Guo, “The principle and state-of-art applications of Hawking radiation,” *J. Phys. Conf. Ser.* **2364**, 012054 (2022).

[18] C. L. Degen, F. Reinhard, and P. Cappellaro, “Quantum sensing,” *Rev. Mod. Phys.* **89**, 035002 (2017), arXiv:1611.02427 [quant-ph].

[19] Stefano Pirandola, Bhaskar Roy Bardhan, Tobias Gehring, Christian Weedbrook, and Seth Lloyd, “Advances in photonic quantum sensing,” *Nature Photon.* **12**, 724–733 (2018), arXiv:1811.01969 [quant-ph].

[20] David DeMille, Nicholas R. Hutzler, Ana Maria Rey, and Tanya Zelevinsky, “Quantum sensing and metrology for fundamental physics with molecules,” *Nature Phys.* **20**, 741–749 (2024).

[21] Carolyn R. Mercer, Erica N. Montbach, Steven D. Christe, Robert M. Connerton, Denise A.

Podolski, Michael P. Robinson, and Mario R. Perez, “Quantum sensing for NASA science missions,” *EPJ Quant. Technol.* **12**, 56 (2025).

[22] Zheshen Zhang and Quntao Zhuang, “Distributed quantum sensing,” *Quantum Sci. Technol.* **6**, 043001 (2021), arXiv:2010.14744 [quant-ph].

[23] M. Płodzień, S. Das, M. Lewenstein, C. Psaroudaki, and K. Roszak, “Harnessing spin-qubit decoherence to probe strongly interacting quantum systems,” *Phys. Rev. B* **111**, L161115 (2025).

[24] A. A. Clerk, M. H. Devoret, S. M. Girvin, Florian Marquardt, and R. J. Schoelkopf, “Introduction to quantum noise, measurement, and amplification,” *Rev. Mod. Phys.* **82**, 1155–1208 (2010).

[25] Kevin C. Young and K. Birgitta Whaley, “Qubits as spectrometers of dephasing noise,” *Phys. Rev. A* **86**, 012314 (2012).

[26] W. G. Unruh, “Absorption cross section of small black holes,” *Phys. Rev. D* **14**, 3251–3259 (1976).

[27] Don N. Page, “Particle emission rates from a black hole: Massless particles from an uncharged, nonrotating hole,” *Phys. Rev. D* **13**, 198–206 (1976).

[28] Sandra Byju, Kinjalk Lochan, and S. Shankaranarayanan, “Quenched Kitaev chain: Analogous model of gravitational collapse,” *Phys. Rev. D* **107**, 105020 (2023), arXiv:1808.07742 [cond-mat.quant-gas].

[29] Greg Kaplanek and C. P. Burgess, “Qubits on the Horizon: Decoherence and Thermalization near Black Holes,” *JHEP* **01**, 098 (2021), arXiv:2007.05984 [hep-th].

[30] Kai Bongs, Simon Bennett, and Anke Lohmann, “Quantum sensors will start a revolution—if we deploy them right,” *Nature* **617**, 672–675 (2023).

[31] Jacob P. Covey, Igor Pikovski, and Johannes Borregaard, “Probing curved spacetime with a distributed atomic processor clock,” *PRX Quantum* **6**, 030310 (2025).

[32] Alexander V. Balatsky, Pedram Roushan, Joris Schaltegger, and Patrick J. Wong, “Quantum sensing from gravity as a universal dephasing channel for qubits,” *Phys. Rev. A* **111**, 012411 (2025).

[33] Matthew D. Horner, Andrew Hallam, and Jiannis K. Pachos, “Chiral Spin-Chain Interfaces Exhibiting Event-Horizon Physics,” *Phys. Rev. Lett.* **130**, 016701 (2023), arXiv:2207.08840 [cond-mat.str-el].

[34] Ewan Forbes, Matthew D. Horner, Andrew Hallam, Joseph Barker, and Jiannis K. Pachos, “Exploring interacting chiral spin chains in terms of black hole physics,” *Phys. Rev. B* **108**, 245142 (2023).

[35] H. T. Quan, Z. Song, X. F. Liu, P. Zanardi, and C. P. Sun, “Decay of loschmidt echo enhanced by quantum criticality,” *Phys. Rev. Lett.* **96**, 140604 (2006).

[36] Ben-Qiong Liu, Bin Shao, and Jian Zou, “Entanglement of two qubits coupled to an  $xy$  spin chain: Role of energy current,” *Phys. Rev. A* **80**, 062322 (2009).

[37] Nitesh Jaiswal, Mamta Gautam, and Tapobrata Sarkar, “Complexity, information geometry, and loschmidt echo near quantum criticality,” *J. Stat. Mech.* **2022**, 073105 (2022).

[38] Nitesh Jaiswal, Mamta Gautam, and Tapobrata Sarkar, “Complexity and information geometry in the transverse  $xy$  model,” *Phys. Rev. E* **104**, 024127 (2021).

[39] S. Santhosh Kumar and S. Shankaranarayanan, “Evidence of quantum phase transition in real-space vacuum entanglement of higher derivative scalar quantum field theories,” *Sci. Rep.* **7**, 15774 (2017), arXiv:1606.05472 [cond-mat.stat-mech].

[40] Revaz Ramazashvili, “Quantum lifshitz point,” *Phys. Rev. B* **60**, 7314–7320 (1999).

[41] Eddy Ardonne, Paul Fendley, and Eduardo Fradkin, “Topological order and conformal quantum critical points,” *Annals of Physics* **310**, 493 – 551 (2004).

[42] E. Fradkin, *Field Theories of Condensed Matter Physics* (Cambridge University Press, 2013).

[43] S. Shankaranarayanan, “Temperature and entropy of Schwarzschild-de Sitter space-time,” *Phys. Rev. D* **67**, 084026 (2003), arXiv:gr-qc/0301090.

[44] Gokhan Alkac and Ege Ozgun, “Simulating hawking radiation in quantum many-body systems: Deviations from the thermal spectrum,” *Phys. Lett. B* **868**, 139783 (2025).

[45] M. L. Mehta, *Random matrices*, 3rd ed., Pure and applied mathematics ; v. 142 (Elsevier/Academic Press, Amsterdam ;, 2004).

[46] W. G. Unruh, “Notes on black-hole evaporation,” *Phys. Rev. D* **14**, 870–892 (1976).

[47] Heinz-Peter Breuer and Francesco Petruccione, *The Theory of Open Quantum Systems* (Oxford University Press, 2007).

[48] W.B. Bonnor, “The hoop conjecture on black holes,” *Phys. Lett. A* **99**, 424–426 (1983).

[49] Jacob D. Bekenstein and Viatcheslav F. Mukhanov, “Spectroscopy of the quantum black hole,” *Phys. Lett. B* **360**, 7–12 (1995), arXiv:gr-qc/9505012.

[50] Bethan Cropp, Swastik Bhattacharya, and S. Shankaranarayanan, “Hints of quantum gravity

from the horizon fluid,” *Phys. Rev. D* **95**, 024006 (2017), [arXiv:1607.06222 \[gr-qc\]](https://arxiv.org/abs/1607.06222).

[51] S. Mahesh Chandran and Uwe R. Fischer, “Expansion-contraction duality breaking in a Planck-scale sensitive cosmological quantum simulator,” *Eur. Phys. J. C* **85**, 1476 (2025), [arXiv:2506.02719 \[gr-qc\]](https://arxiv.org/abs/2506.02719).

[52] L. H. Ford, “Quantum field theory in curved space-time,” in *9th Jorge Andre Swieca Summer School: Particles and Fields* (1997) pp. 345–388, [arXiv:gr-qc/9707062](https://arxiv.org/abs/gr-qc/9707062).